BIOCHEMISTRY
including biophysical chemistry & molecular biology

Article

pubs.acs.org/biochemistry

Standard Role for a Conserved Aspartate or More Direct Involvement in Deglycosylation? An ONIOM and MD Investigation of Adenine–DNA Glycosylase

Jennifer L. Kellie, Katie A. Wilson, and Stacey D. Wetmore*

Department of Chemistry and Biochemistry, University of Lethbridge, 4401 University Drive West, Lethbridge, Alberta, Canada T1K 3M4

Supporting Information

ABSTRACT: 8-Oxoguanine (OG) is one of the most frequently occurring forms of DNA damage and is particularly deleterious since it forms a stable Hoogsteen base pair with adenine (A). The repair of an OG:A mispair is initiated by adenine–DNA glycosylase (MutY), which hydrolyzes the sugar–nucleobase bond of the adenine residue before the lesion is processed by other proteins. MutY has been proposed to use a two-part chemical step involving protonation of the adenine nucleobase, followed by S_N1 hydrolysis of the glycosidic bond. However, differences between a recent (fluorine recognition complex, denoted as the FLRC) crystal structure and the structure on which most mechanistic conclusions have been based to date (namely, the lesion recognition complex or LRC) raise questions regarding the mechanism used by MutY and the discrete role of various active-site residues. The present work uses both molecular dynamics (MD) and quantum mechanical (ONIOM) models to compare the active-site conformational dynamics in the two crystal structures, which suggests that only the understudied FLRC leads to a catalytically competent reactant. Indeed, all previous computational studies on MutY have been initiated from the LRC structure. Subsequently, for the first time, various mechanisms are examined with detailed ONIOM(M06-2X:PM6) reaction potential energy surfaces (PES) based on the FLRC structure, which significantly extends the mechanistic picture. Specifically, our work reveals that the reaction proceeds through a different route than the commonly accepted mechanism and the catalytic function of various active-site residues (*Geobacillus stearothermophilus* numbering). Specifically, contrary to proposals based on the LRC, E43 is determined to solely be involved in the initial adenine protonation step and not the deglycosylation reaction as the general base. Additionally, a novel catalytic role is proposed for Y126, whereby this residue plays a significant role in stabilizing the highly charged active site, primarily through interactions with E43. More importantly, D144 is found to explicitly catalyze the nucleobase dissociation step through partial nucleophilic attack. Although this is a more direct role than previously proposed for any other DNA glycosylase, comparison to previous work on other glycosylases justifies the larger contribution in the case of MutY and allows us to propose a unified role for the conserved Asp/Glu in the DNA glycosylases, as well as other enzymes that catalyze nucleotide deglycosylation reactions.

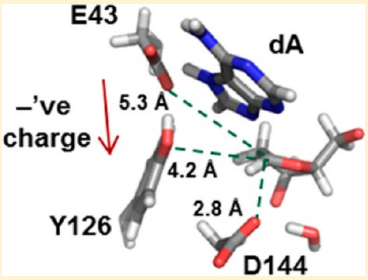

The integrity of the genetic code must be continually protected from various damaging mechanisms including oxidative stress,[1] which has been linked to cancer[2−5] and neurodegenerative diseases.[6−8] One of the most prevalent and stable forms of oxidative damage arises from the conversion of guanine to 7,8-dihydro-8-oxoguanine (8-oxoguanine, OG). Because of similarities between the Hoogsteen face of OG and the Watson–Crick face of thymine, OG can form strong hydrogen-bonding interactions with adenine.[9−11] As a result, polymerases often read OG lesions as thymine residues during replication and preferentially place adenine opposite OG, which can lead to G:C → T:A transversion mutations.[12]

In bacteria, the deleterious effects of the OG lesion are prevented by a collection of proteins that form the GO system, namely, MutM (FPG, EC. 3.2.2.23), MutY (EC. 3.2.2.−), and MutT (EC. 3.6.1.55).[13−15] MutM and MutY are both glycosylases that initiate the base excision repair (BER) pathway by hydrolyzing the sugar–nucleobase N-glycosidic bonds,[16,17] while MutT is a nucleotide sanitization protein.[18,19] Specifically, MutM catalyzes the deglycosylation of OG when base-paired with cytosine.[14] In the event that one round of replication has occurred and an OG:A pair has formed, MutY selectively removes the adenine residue (to be replaced with cytosine by a BER polymerase) in preparation for MutM.[20] However, repairing all adenine mismatches in this way assumes that OG should always be replaced with guanine. Another possibility involves misincorporation of an OG nucleotide opposite adenine, in which case MutY repair would lead to a T:A → G:C transversion. Therefore, a third repair protein, MutT, hydrolyzes the OG nucleotide triphosphate to remove it from the nucleotide pool.[18] Because of their interplay, if any one of these proteins is disrupted, serious downstream implications arise. For example, a common polymorphism of hMYH (the human homologue of MutY) removes OG

Received: September 20, 2013
Revised: October 29, 2013
Published: October 29, 2013

dx.doi.org/10.1021/bi401310w | *Biochemistry* 2013, 52, 8753−8765

specificity and is associated with multiple diseases, such as MYH-associated polyposis (MAP), and has been linked to a predisposition to colorectal cancer.[21,22]

The mechanism of action of MutY has been studied with a variety of methods including kinetics,[20,23−30] alternative substrates,[31−40] kinetic isotope effects,[41] and protein crystallography.[23,26,42−46] Mutational studies have identified two essential catalytic residues: E43 and D144 (*Geobacillus stearothermophilis* numbering used throughout).[23,24,30] Analysis of a crystal structure of OG:A bound to MutY(D144N) (referred to in the literature as the lesion recognition complex, LRC, Figure 1A) indicates that E43 is aligned with N7 of adenine, while

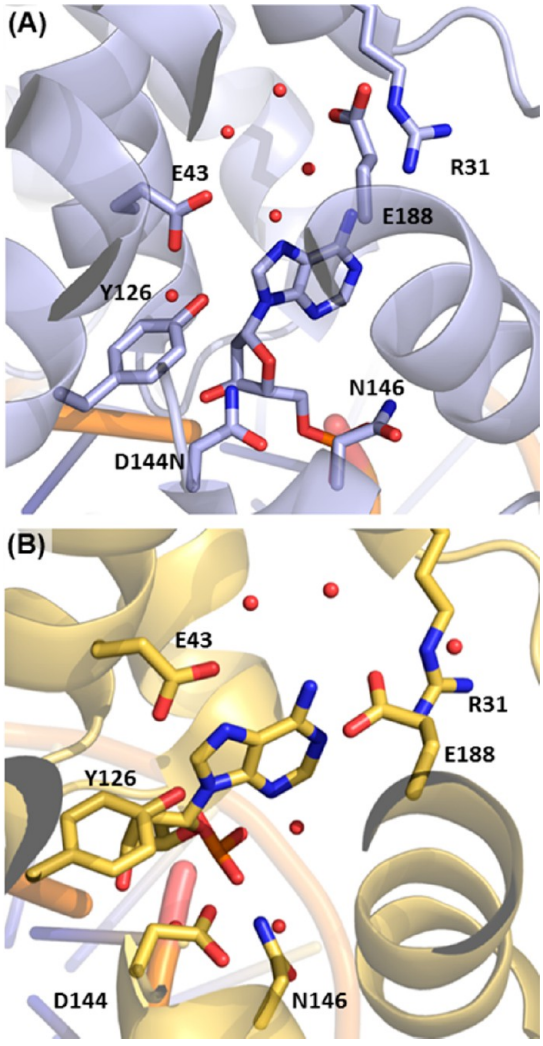

Figure 1. (A) Active site of MutY(D144N) with OG:A bound (LRC, PDB ID 1RRQ). (B) Active site of MutY with OG:FdA bound (FLRC, PDB ID 3G0Q).

D144 is near the deoxyribose ring. The LRC led to the generally accepted mechanism whereby E43 acts as a general acid (via a bridging water molecule) in the first protonation step and as a general base in the second hydrolysis step (Figure 2A).[42] However, due to the lack of direct contacts between MutY and adenine, Verdine et al. later developed a crystal structure of MutY bound to 2′-fluoro-dA (FdA) containing DNA (denoted as the FLRC, Figure 1B).[45] Importantly, the new structure contains direct contacts to FdA. Since experiments show that wild-type MutY binds FdA-containing DNA with the same strength as MutY(D144N) binds dA-containing DNA,[24,34,38] the difference in active-site contacts is likely not due to over-binding of the inhibitor. In addition to proposing that direct contacts with the substrate potentially play a role in catalysis, the FLRC suggests that D144 rather than E43 is aligned to facilitate the reaction as the general base (Figure 2B).

Both of the previously proposed MutY mechanisms are consistent with a wealth of experimental data. Indeed, there is substantial support for an initial dA protonation step. First, kinetic isotope effects indicate that protonation of N7 occurs before deglycosylation.[41] Second, MutY is inactive toward a 7-deaza analogue.[38] Third, E43 is aligned for proton transfer to N7 (either directly[42,45] or indirectly through a bridging water molecule[42]). A recent study found that a carboxyl group is required in the E43 position since an E43D mutant maintains weak activity, but an E43C mutant is inactive.[30] In addition, a pH profile indicates that E43 is initially neutral and that catalytic activity is hindered when the residue is initially anionic.[30] The nonenzymatic depurination of nucleosides and oligonucleotides is known to be acid catalyzed, with protonation of the nucleobase contributing up to 30 kJ mol^{-1}.[41] Therefore, this first step of the reaction may account for almost half of the catalytic activity of the enzyme.[47] Interestingly, there appears to be little leaving group stabilization after the proton transfer step. For example, N1 and N3-deaza-adenine substrates are both catalytically active (albeit at reduced rates),[38,40] which indicates that hydrogen bonding at these sites is not essential. In addition, MutY is active toward a modified substrate with the N6-amine group converted to a methyl group.[38] This activity is supported by KIE results that indicate a hydrogen bond to N6 in the reactant is broken before the depurination transition state.[41]

There is less definitive evidence regarding the hydrolysis step. Measured kinetic isotope effects indicate that the hydrolysis step follows a $D_N{*}A_N^{\ddagger}$ mechanism.[41] In this mechanism, the glycosidic bond breaks in the first, rate-limiting, reversible step (D_N*), and a water molecule adds to the resulting oxacarbenium cation in the final irreversible step ($A_N^{\ddagger}$). Unfortunately, the KIE does not provide explicit evidence indicating which residue (E43 or D144) acts as the general base and activates the nucleophile. However, other glycosylases (such as hUNG2, hOgg1 and AAG) contain a catalytically essential aspartate or glutamate located near the sugar moiety in a similar position as D144 in the FLRC, ideally positioned to act as the general base that activates the water nucleophile.[16,17] Nevertheless, there is no evidence that the water nucleophile in MutY is deprotonated prior to attack on the anomeric carbon. Instead, a leading theory is that the anionic charge on D144 assists stabilization of the cationic intermediate,[30,41] which has similarly been proposed for other glycosylases.[16,17] In the case of MutY, it has recently been shown that an anionic charge in this position is particularly essential for activity since a D144E mutant is catalytically active at wild-type levels and a D144C mutant is active at a pH where the cysteine residue is deprotonated.[30] Regardless, the exact role of D144 in the MutY mechanism is currently unclear.

Computational studies can provide vital molecular level information regarding the role of active-site residues and aid in experimental studies to reveal the mechanism employed by enzymatic systems (see, for example, refs 48−57). However, unfortunately no previous computational study has considered the FLRC crystal structure of MutY or the differences in the associated proposed mechanism (D144 as general base)

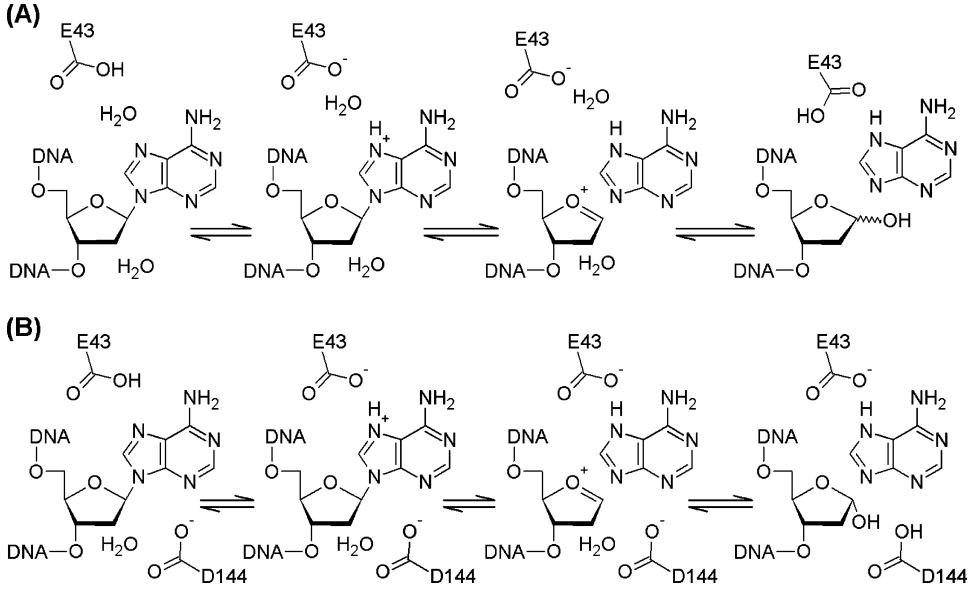

Figure 2. (A) Mechanism based on the LRC, with E43 as the general acid and general base. (B) Mechanism based on the FLRC, with E43 as the general acid and D144 as the general base.

compared to the generally accepted alternative (E43 as general base, Figure 2).[58,59] Therefore, the present work fills an important void in the DNA repair literature by considering the mechanistic implications of the FLRC, with a particular emphasis placed on understanding the essential role of D144. For the first time, a rigorous computational protocol that invokes both molecular dynamics (MD) and quantum mechanical (QM) ONIOM methods is used to compare the dynamical structure of the LRC and FLRC. This analysis questions why all previous computational studies have been initiated from the (LRC) crystal structure. Subsequently, the mechanism employed by MutY is critically analyzed using detailed reaction potential energy surface scans, which have recently been used to gain important insights into the mechanisms of action of other DNA glycosylases, including hUNG2,[60] and AAG.[53] New roles for active-site residues are identified, including the essential function of D144, which is consistent with experimental evidence and justifiably more involved than observed for other glycosylases,[16,17] and the catalytic importance of Y126, which has yet to be acknowledged in the literature. Most importantly, our analysis clarifies a unified role of active-site Asp/Glu residues that are present in many enzymes in the DNA glycosylase family. Our findings also have important implications for the mechanism of action of other enzymes that catalyze nucleoside or nucleotide deglycosylation reactions such as RNA hydrolases, phosphorylases, and glycosidases.

COMPUTATIONAL DETAILS

Molecular Dynamics Simulations. MD simulations were initiated from both the LRC and FLRC crystal structures. PROPKA 3.1[61−64] and chemical intuition were used to assign the initial protonation states of the amino acid R-groups. Notably, E43 was determined to be neutral. Modified residues (8-oxoguanine and N7-protonated adenine) were assigned GAFF[65] and AMBER ff99SB[66] parameters using Antechamber (Tables S1−S5 and Figures S1−S2, Supporting Information),[67] while all other residues were assigned AMBER ff99SB parameters. Partial charges were obtained from HF/6-31G(d) using Gaussian 09 (revision A.02)[68] and RESP charge fitting with the R.E.D.v.III.4 program.[69] Parameters for the iron−sulfur cluster were adapted from the literature.[70,71] Missing and partially resolved residues were added using overlays of the 3FSP crystal structure, and mutations were reverted. Both systems were neutralized with sodium ions and solvated in an 8.0 Å (105 Å × 105 Å × 105 Å) TIP3P water box using the LEaP module of AMBER 11, with initial minimizations of the solvent and ions conducted while applying a 500 kcal mol^{-1} constraint on the enzyme and DNA. Subsequently, 1000 steps of unrestrained steepest descent and 1500 steps of unrestrained conjugate-gradient minimization were performed on the entire system. The system was then heated at constant volume from 0 to 300 K over 20 ps with a 10 kcal mol^{-1} restraint on all DNA and protein atoms. The entire system was then simulated without restraints for 20 ns (LRC) or 40 ns (FLRC) at 300 K and 1 atm. All simulations used a 2 fs time step and were conducted using the SANDER module of AMBER 11[72] or 12,[71] while trajectory analysis was completed using the ptraj module of AMBER 11. Additional details of the MD simulation protocol are provided in the Supporting Information.

Quantum Mechanical Model. *Reactant Generation.* Following a detailed comparison of the LRC and FLRC (see Results), the FLRC[45] was used as the starting point for all quantum mechanical models. The enzyme−substrate complex was generated by first selecting a 10 Å sphere around the FdA residue (A5L18) (Table S6, Supporting Information). The charge of the full system is −5 with 838 total atoms (424 heavy atoms). Truncation points were capped with hydrogen atoms constrained to the crystal structure orientation of the replaced atom. The remaining hydrogen atoms were added manually to maximize hydrogen-bond contacts and optimized with PM6 while fixing the heavy atom positions. Finally, the system was relaxed using ONIOM(M06-2X/6-31G(d):PM6) with the low-level region held fixed. The DFT region contains all groups that directly interact with adenine or the proposed nucleophile, namely, the FdA nucleoside, waters 28, 50 and 371, and the functional groups of R31, E43, Y126, D144, N146, and E188 (Figure 3 and Table S6, Supporting Information). The

dx.doi.org/10.1021/bi401310w | *Biochemistry* 2013, 52, 8753−8765

corresponding DFT region contains 104 total atoms (54 heavy atoms) and a charge of −1.

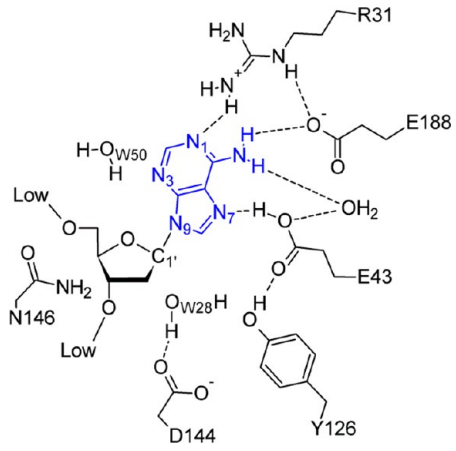

Figure 3. Schematic of the residues included in the DFT region of the various ONIOM models.

Conformational Search. A conformational search of selected residues in the MutY active site was carried out with the ONIOM model generated from the FLRC. Initially, each dihedral angle in the R-groups of the residues of interest was modified in 60° increments, and conformations with small interatomic distances were removed. Next, single-point energy calculations were carried out on each conformation with PM6. Structures within 100 kJ mol^{-1} of the most stable conformer were then relaxed with our ONIOM(M06-2X/6-31G(d):PM6) model. At this point, the resulting geometries for the each set considered were combined, such that each residue adopted the most energetically feasible orientation, and the resulting structure was reoptimized with ONIOM.

Reactions. Using our ONIOM(M06-2X/6-31G(d):PM6) model generated from the FLRC as described in the Reactant Generation subsection, two possible mechanisms of action of MutY were studied using reaction potential energy surface scans. The first step in the MutY reaction, transfer of a proton from E43 to N7, was modeled by scanning the $O\varepsilon_{E43}$−H distance. The hydrolysis step was modeled from the fully relaxed activated reactant with the proton on adenine (RC*). Specifically, two-dimensional reaction PES were generated with the glycosidic bond (C1′−N9) as one coordinate and the nucleophile attack distance (C1′−O_{nuc}) as the second coordinate. Minima for productive mechanisms were fully relaxed (constraints on the glycosidic bond and nucleophile distance removed), and the transition states were further refined to a 0.050 Å grid. The DFT regions were extracted from the stationary points, and M06-2X/6-31G(d) frequency calculations were carried out to obtain estimates of the zero-point vibrational energy and thermal correction to Gibbs energy, as well as to verify the nature of stationary points.[55−57] Although the stationary points identified from the PES may have more than one imaginary frequency due to the structural constraints imposed, we note that a significant imaginary frequency that corresponds to the reaction pathway can be identified for all transition states (see coordinates for the DFT region of the refined stationary points in the Supporting Information). Furthermore, a previous study on another DNA glycosylase (AAG) has verified that stationary points identified from PES scans are excellent (structural and energetic) approximations of the corresponding fully optimized geometries.[53] High-quality energetics for the refined stationary points were obtained with ONIOM(M06-2X/6-311+G(2df,2p):PM6).

All QM calculations were carried out with Gaussian 09 (revisions A.02 and C.01).[68] Full computational details are provided in the Supporting Information.

RESULTS

Critical Comparison of Crystal Structures. As mentioned in the first section, there are two primary crystal structures that have yielded important insight into the mechanism of action of MutY (denoted LRC and FLRC, Figure 1). Despite the fact that all previous computational studies on MutY have been initiated from the LRC,[58,59] the crystal structure of this (D144N) mutant does not contain direct contacts between the protein and adenine substrate. Consistent with previous literature,[59] a significant amount of water remains in the active site following MD simulations initiated from the LRC (Table 1 and Figures 4A and S3−S7, Supporting Information). Furthermore, the active-site waters form close contacts with the adenine substrate (Tables S7−S9, Supporting Information). Most importantly, these interactions prevent direct contacts between the substrate and accepted catalytically essential residues, such as E43. In fact, hydrogen-bonding occupancies (Tables S8 and S9, Supporting Information) suggest that only six hydrogen-bonding interactions exist between any two active-site residues (none with dA), with the largest occupancy of 56% of the simulation time.

Overall, MD simulations initiated from the FLRC exhibit much less water in the active site than those initiated from the

Table 1. Summary of MD Results[a]

	LRC	FLRC	FLRC	FLRC
	dA	dA	dA^{7H}	dA^{7H}
model	cap	cap	cap	nocap
water molecules within 3.6 Å of dA(C1′)	7.8 (3.1)	2.2 (0.7)	0.1 (0.3)	1.0 (1.0)
E43(Oδ1)···dA(N7) distance (Å)	4.514 (0.360)	4.790 (1.326)	2.926 (0.161)	2.728 (0.092)
D144 Cα-Cβ-Cγ-Oδ1 dihedral (deg)[b]	221.5 (116.1)	173.2 (98.6)	231.8 (11.9)	118.7 (30.4)
D144(Oδ1)···V147(NH) distance (Å)	4.143 (0.850)	4.881 (0.984)	2.876 (0.131)	5.273 (1.395)
Y126(OH)···E43(Oε1) distance (Å)	3.833 (0.599)	4.916 (0.688)	2.633 (0.102)	2.663 (0.218)
dA sugar pseudorotation values (deg)	89.9 (50.6)	117.1 (75.2)	334.2 (18.4)	262.5 (116.5)
E188 Cα-Cβ-Cγ-Cδ dihedral (deg)[c]	228.2 (88.4)	195.9 (66.4)	243.8 (88.2)	197.1 (67.7)

[a]Average number, distance, or angle (standard deviation). [b]Helix-capping interaction occurs at ∼155° and 206°. [c]Original dihedral was 160° and 75° in the LRC and FLRC, respectively.

dx.doi.org/10.1021/bi401310w | *Biochemistry* 2013, 52, 8753−8765

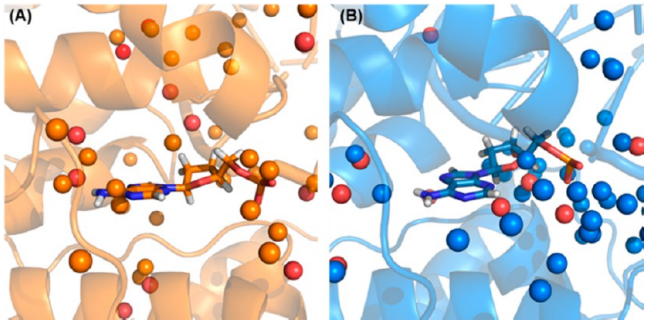

Figure 4. Distribution of crystallographic (red) and solvent box (orange or blue) water in the (A) LRC and (B) FLRC active sites in the crystal structure (orange or blue) and after a 20 ns MD simulation with (neutral) dA bound.

LRC (Table 1 and Figures 4 and S3–S7, and Table S7, Supporting Information). As a result, a direct contact between dA and E43 is present for approximately 60% of the FLRC simulation (Table S8 and Figure S8, Supporting Information), which is consistent with the observed specificity of MutY.[38] Furthermore, four additional direct contacts are formed between active-site residues with occupancies of 35–95% (Table S8 and S9, Supporting Information), which in conjunction with the spread in the distributions of bond lengths and dihedral angles (Figures S8–S11, Supporting Information) suggests more specific binding of the substrate in the FLRC. In addition to a significant difference in the location of E43 in the LRC and FLRC crystal structures and simulations (Figures 1 and 5), D144 is less mobile in the FLRC than in the

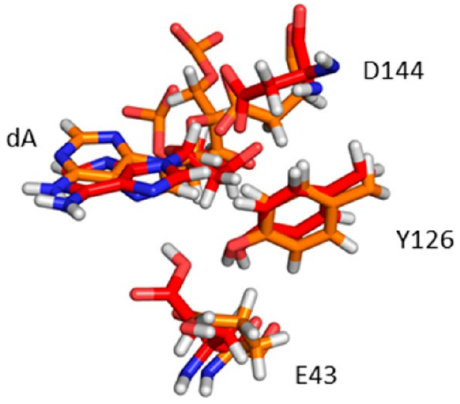

Figure 5. Overlay of representative structures from MD simulations of the LRC (orange) and FLRC (red) crystal structures with (neutral) dA bound in the active site.

LRC simulation (the RMSF of D144 is 0.755 and 0.553 in simulations initiated from the LRC and FLRC, respectively; see also the standard deviation of the D144 dihedral in Table 1 and Figures S9–S10 and Table S9, Supporting Information). As a result, D144 is in a location similar to that of other glycosylases[16,17] and is likely poised for catalysis in the FLRC, while this residue is not in a catalytically competent location in the LRC crystal structure[42] or simulation.

The above results suggest that the lack of specific contacts with the substrate in the LRC but the presence of these contacts in the FLRC, is maintained upon consideration of the dynamics of the active site. However, the difference in active-site contacts is likely not due to over-binding of the inhibitor (MutY:FdA and MutY(D144N):dA have similar binding strengths).[24,34,38] On the basis of the presence of direct substrate contacts, the FLRC provides a closer representation of the catalytically competent reactant complex than the LRC. Indeed, an overlay of the active sites of the LRC, FLRC, and a product complex (PDB ID 1VRL) indicates that the FLRC bears a stronger resemblance to the product (RMSD = 0.593 Å) than the LRC does (RMSD = 0.920 Å, and Figure S12, Supporting Information). Therefore, a reactant based on the FLRC would require the least atomic motion to proceed through the reaction and is the focus for further computational investigation. From a computational point of view, the FLRC is also a more logical starting point for modeling since this structure contains no active-site mutations, and the inhibitor should cause minimal changes to the active-site fold. Thus, although all previous computational studies have been initiated from the LRC,[58,59] considering other computational starting points is critical for an accurate analysis. In the case of MutY, the large change in the relative orientation of active-site residues (e.g., E43 and D144) with respect to the adenine substrate in the FLRC and LRC (compare Figure 1A and B) suggests that the previous computational studies based on the LRC could characterize a different mechanism of action than those initiated from the FLRC. Therefore, the present work focuses on the mechanistic implications of the FLRC.

Active-Site Dynamics Following Substrate Activation. Since there is substantial experimental evidence for an initial nucleobase protonation step prior to deglycosylation,[30,38,41] the effect of direct proton transfer from E43 to N7 of dA (dA^{7H}) on the active-site structure and dynamics was considered based on the FLRC. When dA is protonated, there is less water in the active site (Tables 1 and S10 and Figures S3–S7, Supporting Information) and, as a result, the active site is tightened upon formation of dA^{7H} (see, for example, Figures S8–S11, Supporting Information). Indeed, a direct contact between (anionic) E43 and (cationic) dA^{7H} is occupied for close to 100% of the simulation, which is significantly higher than the occupancies for substrate interactions when dA is neutral (Table S8, Supporting Information). Furthermore, a high (100%) occupancy hydrogen bond is formed between the R-groups of E43 and Y126, which holds dA, E43, and Y126 in close proximity and is in stark contrast to the weaker Y126 interaction with the backbone carbonyl of E43 when dA is neutral (E43(Oδ1)···dA(N7) distance in Table 1; see also Table S8 and Figure S11 and S13, Supporting Information). Interestingly, the puckering of the deoxyribose moiety changes upon protonation of dA to the C3′–*exo* conformation anticipated based on experimental evidence[45] (Table 1 and Figure S15, Supporting Information). In the FLRC crystal structure, D144 caps the helix of the MutY HhH motif through a hydrogen bond to V147 (Figure S14, Supporting Information). Although D144 interacts with N146 in the MD simulations regardless of the protonation state of dA (N_{N146}–H···Oδ_{D144}), the helix-capping interaction with V147 is only present in the FLRC when dA is protonated ((N_{V147}–H···Oδ_{D144}) in Table 1 and S9 and Figure S9–S10, Supporting Information), which would provide additional stability to the active site. Combined, these MD results support experimental suggestions that dA is protonated in the active site in a step prior to deglycosylation.

Orientation of Active-Site Residues. Because of the potential role of D144 as a general base in the mechanism of MutY action, it is important to further consider the dynamic

dx.doi.org/10.1021/bi401310w | *Biochemistry* 2013, 52, 8753–8765

orientation of this residue in the active site after dA protonation has occurred. Specifically, since D144 was found to adopt several conformations in the simulations, an additional simulation was initiated with the N_{V147}−H···Oδ_{D144} helix-capping interaction broken through the rotation of the D144 R-group. In this simulation, the helix-capping interaction is occupied for 65% of the simulation (Table S9, Supporting Information). Furthermore, the helix cap was present at the start of the production run but breaks halfway through and remains broken during the rest of the simulation. Therefore, the effect of this helix-capping interaction should be considered when contemplating a mechanism of action of MutY since this role for D144 may be loosely defined, and D144 may be able to actively participate in the deglycosylation reaction. For example, breaking the helix cap would increase the basicity of D144, which would increase its ability to activate the water nucleophile during deglycosylation. It is also important to note that, in all simulations, E188 adopts an orientation that is different from the published structure[45] but better reflects the electron density of the FLRC (Table 1 and Figure S16, Supporting Information).

Because of the observed dynamics of certain active-site residues, the conformational landscape of the active site was further analyzed with QM using an ONIOM model generated from the FLRC in order to gain information about the relative energy of potentially important conformations. Initially, the conformations of D144 and N146 were jointly considered because of their role in the formation of the helix cap, and two conformations were identified following ONIOM relaxations of the 13 lowest energy structures from a preliminary (PM6) search. The lowest energy conformation maintains the helix-capping interaction between D144 and the backbone amide of V147 observed in the X-ray crystal structure, while the other orientation breaks this contact at a cost of 51.6 kJ mol^{-1}. Subsequently, the orientations of E188 and R31 were jointly considered due to differences in the simulation and published FLRC structures. Nine conformations of R31 and E188 were obtained with ONIOM after the relaxation of 30 orientations from the preliminary search. Notably, 19 of the 30 conformations fell to the lowest energy structure in which E188 adopts a conformation consistent with MD and the experimental electron density of the FLRC (Figure S17, Supporting Information). A structure that resembles the reported FLRC geometry was also obtained and was 66.1 kJ mol^{-1} higher in energy. When the two D144/N146 and nine R31/E188 conformations were combined and relaxed with ONIOM, the energetic differences observed in the separate optimizations were maintained.

An overlay of the heavy atoms in the ONIOM reactant and the equivalent atoms in a representative structure from the FLRC simulation (with the helix cap in place) shows that both methods result in the same active-site geometry (RMSD = 0.978 and 0.672 Å for all heavy atoms and just the DFT region, respectively, Figure 6). Therefore, several ONIOM models were confidently used to study the reaction mechanism and clarify the role of select amino acids (Table 2).

Mechanism Catalyzed by MutY. *Proton Transfer.* Since experimental[41] and MD (above) evidence supports an initial proton transfer step, transfer from E43 to dA was modeled prior to considering deglycosylation. On the basis of the surfaces for the three models (Figure S18, Supporting Information), proton transfer is calculated to be barrierless and likely does not contribute to the total reaction barrier. After

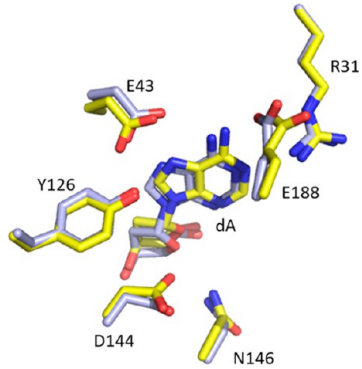

Figure 6. Overlay of all heavy atoms in the MutY ONIOM active-site model obtained with MD (representative structure from FLRC simulation with N7-protonated dA bound, light blue) and QM (RC* with CS-Cap model, yellow). (For clarity, only atoms included in the DFT region are shown.)

Table 2. Summary of the ONIOM Models Used in the Present Study

model	D144[a]	E188[b]
X-WT	helix cap	FLRC[c]
CS-Cap	helix cap	alternate[d]
CS-NoCap	broken cap	alternate[d]

[a]Orientation of D144. [b]Orientation of E188. [c]Conformation from the FLRC crystal structure.[45] [d]Orientation from the QM conformational search, see Computational Details.

proton transfer, slight elongation of the glycosidic bond (by up to 0.021 Å) is observed, which is consistent with the effect of N7 protonation on nucleotide structures.[73−75] Although a previous large-model computational study observed proton transfer concomitant with depurination,[59] proton transfer could not occur earlier due to the methodology implemented. In contrast to the generally accepted MutY mechanism based on the LRC, the barrierless proton transfer calculated with the ONIOM models coupled with the results from the MD simulations suggests that the primary role of E43 is direct protonation of the nucleobase (rather than protonation through a water molecule) and that the protonation step occurs prior to glycosidic bond cleavage. Furthermore, these results indicate that the adenine substrate is protonated in the FLRC crystal structure.

Standard Hydrolysis. In the standard hydrolysis mechanism based on the FLRC (Figure 2B), a water molecule (Wat28) below the plane of the sugar moiety acts as the nucleophile, which can be activated by D144 through either hydrogen bonding or full proton transfer. In the calculated reaction PES (Figure 7), the reactant well occurs in the bottom left corner, deglycosylation occurs along the horizontal axis, and attack on the anomeric carbon occurs on the vertical axis. The X-WT model, which uses the published FLRC X-ray crystal structure conformation of the active site, leads to a large barrier (ΔE = 150.6 kJ mol^{-1}) to deglycosylation (TSD, Table 3) and does not proceed to products (Figure 7A). Therefore, it is important to consider alternate active-site geometries identified from MD or ONIOM and not solely rely on published X-ray structures.

MD and ONIOM conformational searches revealed an alternate conformation of E188 (with D144 remaining in a helix-capping position) and was used to generate the CS-Cap model. In contrast to the X-WT model, products are obtained

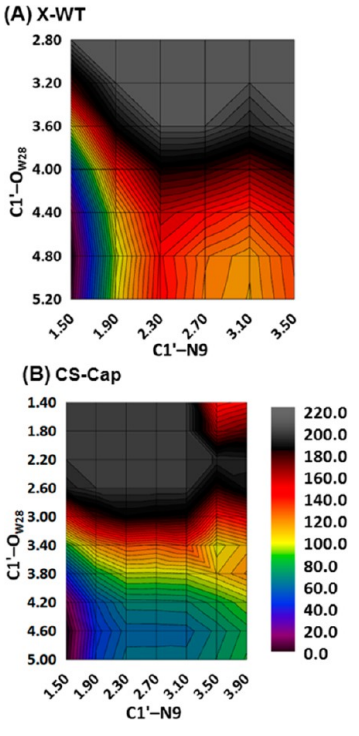

Figure 7. ONIOM(M06-2X/6-31G(d):PM6) reaction PES (kJ mol^{-1}) for the standard hydrolysis with the (A) X-WT and (B) CS-Cap models. Each contour represents 5 kJ mol^{-1}.

Table 3. Summary of ONIOM Reaction Energetics (kJ mol^{-1}) Estimated from Reaction Potential Energy Surfaces and Relaxed Stationary Points[a]

mechanism	model	RC*	TSD	IC	TSA	PC
Reaction Potential Energy Surfaces[b]						
standard hydrolysis	X-WT	0.0	150.6	112.7	NR[c]	NR[c]
	CS-Cap	0.0	63.8	60.5	201.0	129.2
D144 dependent	CS-Cap	0.0	35.1	19.6	148.1	105.1
	CS-Nocap	0.0	30.5	14.3	97.5[d]	54.5[d]
Relaxed Stationary Points[e]						
D144 dependent	CS-Cap	0.0	30.9 (32.0)	7.8 (10.0)	156.7 (168.1)	104.4 (113.3)
	CS-NoCap	0.0	30.6 (31.1)	11.5 (17.7)	110.0[d] (115.8)	57.7[d] (61.0)
Y126F Mutant[e,f]						
D144 dependent	CS-Cap	0.0	38.5 (42.2)	19.8 (24.8)	165.5 (171.5)	115.0 (113.7)
	CS-Nocap	0.0	34.1 (29.7)	23.1 (23.9)	122.0[d] (125.4)	71.5[d] (67.6)

[a]ONIOM(M06-2X/6-31G(d):PM6) geometries. See Computational Details for model specifications. [b]Optimization level energies. [c]No reaction observed. [d]Geometry from the CS-Cap surface. [e]ONIOM-(M06-2X/6-311+G(2df,2p):PM6) single-point energies with ZPVE corrections included (Gibbs energies are in parentheses). [f]See the full computational details in the Supporting Information for additional details on the mutant calculations.

with the CS-Cap model (Figure 7B). In addition, the barrier to deglycosylation is reduced by over half (ΔE = 63.8 kJ mol^{-1}, Table 3), but addition of the water nucleophile to the anomeric carbon is still high in energy (ΔE = 201.0 kJ mol^{-1}). Therefore, this modification of the published active-site conformation is not enough to make the standard hydrolysis mechanism viable. Nevertheless, analyzing the reaction will allow for a better understanding of how MutY functions. For example, the large barrier for nucleophilic attack at C1′ may arise in part since the proposed general base (D144) is involved in multiple hydrogen-bonding interactions with the backbone of V147 (X-WT, CS-Cap models), the R-group of N146 (CS-Cap) and/or the hydroxyl group of Y126 (X-WT). However, there is a large migration of D144 in the active site throughout the reaction (for example, the distance between C1′ and a carboxyl group of D144 decreases by over 0.4 Å for the CS-Cap model due to mutual migration of both groups), which suggests that the orientation of this residue should be further considered.

Contrary to previous computational studies based on the LRC, E43 is not directly involved in the deglycosylation reaction when the FLRC is considered. However, E43 is coupled to Y126. Furthermore, alternate binding modes of Y126 to E43 were observed in the MD simulations, and significant motion of Y126 was observed (by over 0.6 Å) over the course of the CS-Cap standard hydrolysis reaction. This hints that the hydroxyl group on Y126 may contribute to catalysis. Part of this catalytic effect likely arises due to stabilization of the E43 anion. However, as the hydrogen bond between Y126 and E43 tightens, the anionic charge on E43 partially delocalizes onto Y126, which brings the anionic charge closer to the cationic sugar. Indeed, d(C1′−O$_{Y126}$) decreases by 0.658 Å during the course of deglycosylation in the CS-Cap model. Therefore, a second potential role for Y126 is stabilization of the charged oxacarbenium intermediate.

D144-Dependent Hydrolysis. The spontaneous movement of D144 noted during depurination in the standard hydrolysis mechanism led us to investigate a new mechanism in which D144 is more directly involved in the deglycosylation step. The CS-Cap model was initially considered for this new mechanism since it exhibits a lower standard hydrolysis barrier than the X-WT model, and MD supports the stability of this active site conformation. In this so-called D144-dependent hydrolysis mechanism, the effect of D144 motion toward the sugar moiety on the dissociation microstep is explicitly considered using the glycosidic bond and C1′−Oδ_{D144} distances as the reaction coordinates in the first (deglycosylation) step. A covalent link between the sugar and D144 was not observed to form on the CS-Cap surface, and therefore the glycosidic bond and C1′−O$_{Wat28}$ distances are the coordinates in the second (nucleophile addition) step (Figure 8).

In the first step of the D144-dependent reaction, the distance between C1′ and Oδ_{D144} reduces from 3.400 Å to 2.600 Å as the dA nucleotide is deglycosylated on the CS-Cap surface (Figures 8A and 9), which weakens the helix-capping interaction (d(N$_{V147}$−H···Oδ_{D144}) = 1.925−2.016 Å; Figure S20H, Supporting Information). The tight contact between the sugar moiety and D144 stabilizes the sugar, and therefore, the deglycosylation barrier characterized for the D144-dependent mechanism (ΔE = ∼31 kJ mol^{-1}) is half that obtained for the standard hydrolysis mechanism, suggesting that this is a more likely mechanism.

MD simulations and QM conformational searches reveal that the active site can adopt a stable conformation when the D144 helix-capping interaction is broken (Table S9, Supporting Information). Since the D144-dependent reaction requires significant motion in this residue, it is possible that starting from a reactant without this contact may reduce the hydrolysis barrier. In addition, D144 should be a stronger general base without the helix-capping interaction. Therefore, the D144-

dx.doi.org/10.1021/bi401310w | *Biochemistry* 2013, 52, 8753−8765

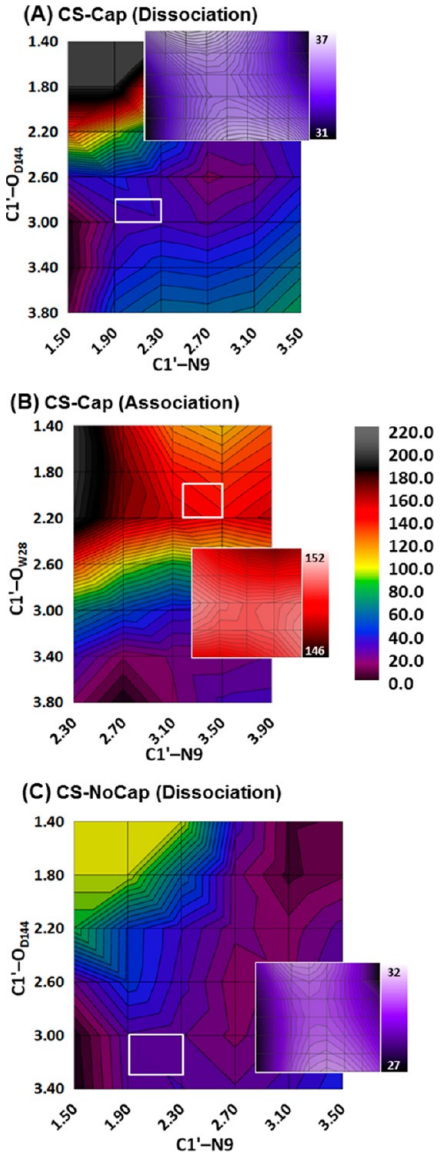

Figure 8. ONIOM(M06-2X/6-31G(d):PM6) reaction PES (kJ mol^{-1}) for the (A) CS-Cap dissociative step, (B) CS-Cap associative step, and (C) CS-NoCap dissociative step of the D144-dependent mechanism with refined regions near the TS inset. Each contour represents 5 kJ mol^{-1} on the 0.4 Å surfaces and 0.15 kJ mol^{-1} on the 0.05 Å inset surfaces.

dependent mechanism was investigated using a model that does not contain the N_{V147}−H···Oδ_{D144} hydrogen bond (CS-NoCap, Table 2). Removing the helix-capping interaction shifts the deglycosylation transition state slightly earlier (d(C1′−Oδ_{D144}) = 2.850 and 3.150 Å for the CS-Cap and CS-NoCap models, respectively; Figure 9) but has no effect on the energetics (Table 3). Interestingly, a stable intermediate is found for both (CS-Cap and CS-NoCap) models with a relative energy of 7.8−11.5 kJ mol^{-1} (Table 3). These energetics, coupled with the fact that the helix cap is easily broken under the constraints of standard MD simulations, suggest that either mechanism is plausible.

The N6 amine of adenine hydrogen bonds with E188 and a water molecule (Wat371). Both interactions tighten near the transition state, then loosen again near the deglycosylated intermediate (Figures S20B and S20D, Supporting Information), which is consistent with KIE data.[41] The only other hydrogen bond to the adenine nucleobase is a contact between N1 and R31, which tightens to ∼1.8 Å at the transition state and then weakens (Figure S20B, Supporting Information). While hydrogen-bonding interactions at N1 may not be necessary for MutY activity,[38,40] the leaving group stabilization provided by such contacts should be catalytic.[76] Following the deglycosylation TS, D144 in the CS-NoCap model becomes unstable and can reform the backbone interaction to V147. Therefore, the water association step was only modeled with the CS-Cap model (Figure 8B), and the energies of the stationary points are reported relative to the corresponding reactants for the CS-Cap and CS-NoCap models (Table 3). From the refined stationary points, the ΔE for the addition of Wat28 to C1′ is 110.0 kJ mol^{-1} relative to the CS-NoCap reactant and 156.7 kJ mol^{-1} relative to the CS-Cap reactant. The barrier to water addition may be reduced if the adenine nucleobase were to dissociate prior to nucleophilic attack on the anomeric carbon, which is supported by adenine release being faster than DNA release.[77]

The intermediate well connecting the dissociation surface to the water association surface (Figure 8B) is quite broad. Indeed, if Wat28 is moved slightly further from the anomeric carbon (and the C1′−N9 distance is increased slightly), a second intermediate can be obtained that is exothermic relative to RC*. Other deglycosylation reaction surfaces have demonstrated stabilization of the system upon partial dissociation of the nucleophile from the active site.[53,60] The fact that an exothermic intermediate is only obtained when the potential nucleophile begins to dissociate from the active site indicates that the MutY active site is ideally formed to stabilize the unstable oxacarbenium cation intermediate. These results are consistent with evidence that release of adenine is faster than DNA release[77] and that the product-bound complex only attributes 30% of the AP-site density to a bound conformation.[42]

Interestingly, the d(C1′−O$_{Y126}$), which was observed to decrease in the standard mechanism, actually increases when D144 is more directly involved in the reaction in both the CS-Cap and CS-NoCap models (Figure S20E, Supporting Information). This observation supports a proposal that the primary catalytic role of Y126 is likely stabilization of the charge generated on E43 in the first (proton transfer) chemical step rather than stabilizing the sugar cation. To discern the magnitude of the catalytic role of this residue, a Y126F mutant was considered (Table 3). The barrier to nucleobase departure increases by up to 10 kJ mol^{-1}, while the barrier to nucleophilic attack increases by up to 12 kJ mol^{-1}, with respect to the corresponding reactant upon consideration of the mutation depending on which model is considered. This suggests that the stability provided by interactions with Y126 changes not only the geometry of the active site but also the overall reaction energetics, which further testifies to the potential importance of this residue.

DISCUSSION

Proposed Mechanism of Action. Following detailed (MD) analysis of available crystal structures for MutY, it was determined that the FLRC, rather than the most widely studied (LRC) structure, leads to a catalytically competent reactant, which unlike the LRC suggests specific contacts to the substrate are formed upon binding and proposes that D144 (rather than E43) is the general base (activates the water nucleophile). Since

dx.doi.org/10.1021/bi401310w | Biochemistry 2013, 52, 8753−8765

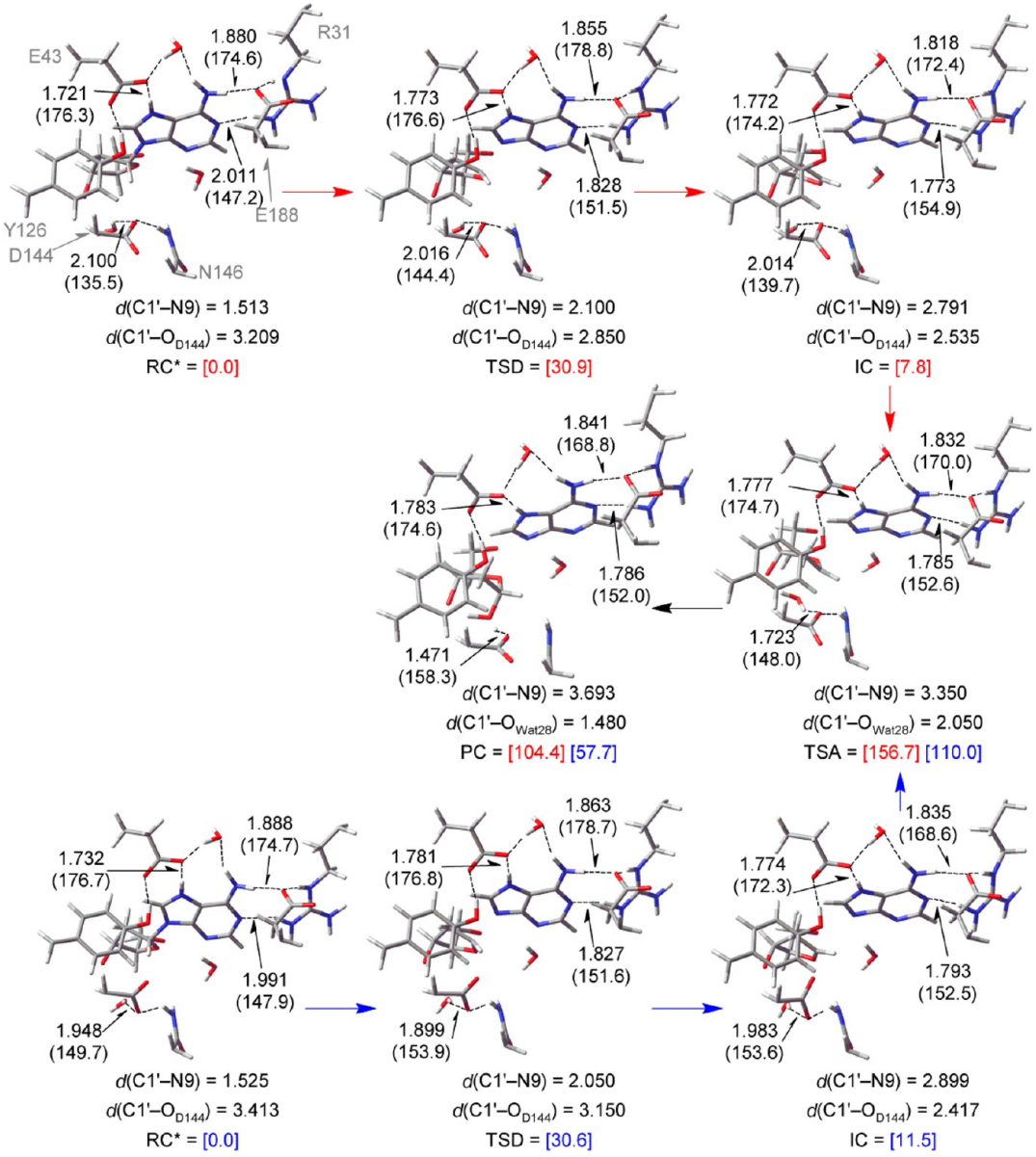

Figure 9. DFT region of the refined stationary points for the D144-dependent hydrolysis with the CS-Cap (upper, red arrows) and CS-NoCap (lower, blue arrows) models. Selected ONIOM(M06-2X/6-31G(d):PM6) distances (Å) and angles (degrees, in parentheses) are shown. ONIOM(M06-2X/6-311+G(2df,2p):PM6) energies (kJ mol^{-1}) relative to the respective reactants (RC*) are in square brackets.

previous computational work on MutY has been solely initiated from the LRC, our analysis suggests that considering different computational starting points may significantly extend the mechanistic picture currently available for MutY. Therefore, the mechanism of action of this important repair enzyme was critically evaluated for the first time using sophisticated computational approaches based on the newest FLRC structure. Detailed reaction potential energy surfaces characterized two potential mechanisms for depurination of dA by MutY. Both mechanisms begin with barrierless proton transfer from E43 to N7 of adenine, which is justified by experimental data and supported by the greater stability of the enzyme–substrate complex with protonated dA over neutral dA according to MD simulations. This finding suggests that the primary role of E43 is nucleobase activation. Subsequently, the lowest energy mechanism involves S_N1 depurination and more significant involvement of D144 than even suggested from the FLRC as evident by significant migration toward the sugar moiety during the deglycosylation step. Within this scheme, the helix cap involving D144 can either remain intact or break during the reaction.

Unlike other glycosylases, such as AAG,[47] experimental estimates of the ΔG for the chemical step are not currently available. However, $\Delta G^{\ddagger}$ can be estimated through comparison of several pieces of experimental data in order to validate our computational model. Specifically, comparing the rate of MutY activity ($0.2\ s^{-1}$)[28,38] to the uncatalyzed hydrolysis of dA ($6.8 \times 10^{-10}\ s^{-1}$)[47] yields a relative rate of 2.9×10^{8} at 37 °C and a corresponding barrier reduction of ~50 kJ mol^{-1}. Combining the barrier reduction with the uncatalyzed hydrolysis barrier (~130 kJ mol^{-1})[47] leads to an estimated experimental $\Delta G^{\ddagger}$ for MutY of ~80 kJ mol^{-1}. It must be acknowledged that the rate-limiting associative barrier calculated in the present work is likely overestimated since the proposed general base (D144) is involved in numerous hydrogen bonds that reduce its ability to accept a proton from the nucleophile, while release of the

dx.doi.org/10.1021/bi401310w | *Biochemistry* 2013, 52, 8753–8765

adenine nucleobase could increase the solvent accessibility of C1′ and thereby lower the barrier to water attack. With this in mind, the estimated experimental barrier reasonably compares to the lowest energy associative barrier ($\Delta G^{\ddagger}$) for the D144-dependent pathway (98.5 kJ mol^{-1} relative to the relaxed intermediate or 115.8 kJ mol^{-1} relative to the reactant, Table 3). Combined with the low-barrier deglycosylation step ($\Delta G^{\ddagger}$ = 31.1−32.0 kJ mol^{-1}), our calculations suggest that the newly proposed D144-dependent pathway is the most likely mechanism of action for MutY, which is consistent with a wealth of experimental data including the relatively new, yet under studied, catalytically competent FLRC structure.

Role of Y126. For the first time, a potential catalytic role of Y126 has been identified. First, MD simulations showed significant variations in the interaction between Y126 and E43 with the dA substrate protonation state. Second, ONIOM calculations suggest that a Y126F mutant increases the reaction barrier for the preferred D144-dependent mechanism. Together, these results lead us to propose that Y126 may contribute to the efficiency of MutY. The primary role of Y126 is likely to stabilize the proton transfer step through a strong hydrogen bond to E43, which alleviates the developing negative charge on this residue. A possible secondary role of Y126 may be to assist the stabilization of charge developed in later reaction steps. For example, transition state stabilization by Y126 could occur in the deglycosylation step through hydrogen bonding with active-site anionic residues, such as E43, which draws the negative charge closer to the cationic sugar moiety. Interestingly, a glutamate−tyrosine dyad can also be found in AAG, which may perform a similar function.[78,79] The role of Y126 in MutY, as well as similar residues in other enzymes, should be carefully considered in future experimental studies.

Role of D144. In the literature, D144 is generally proposed to provide electrostatic stabilization to the deglycosylation transition state, while the FLRC suggests that D144 (rather than E43 as suggested by the LRC) may act as a general base to activate the nucleophile.[16,17] These roles for D144 are primarily based on the observed catalytic contribution of active-site Asp/Glu residues in similar locations in other glycosylases, such as UDG (hUNG2), hOgg1, NEIL1, AlkA, and AAG.[16,17] Our newly proposed mechanism provides the first computational support for these roles. In addition, we propose that D144 plays an even more explicit role than has been previously discussed for this (or similar) residue(s) in other glycosylases. Specifically, the distance between C1′ and the D144 functional group decreases substantially during deglycosylation in all mechanisms and models investigated. Previous studies on DNA glycosylases have not proposed significant migration of the active-site aspartate residue.[16,17,53,60,80]

In contrast to other glycosylases (such as hUNG2), MutY excises a cationic nucleobase, which results in a neutral leaving group. This is a crucial difference from the reaction catalyzed by other glycosylases since the negatively charged nucleobase near the oxacarbenium intermediate has been removed, which has been implicated as an important part of the electrostatic sandwich that stabilizes the cation. For example, the oxacarbenium cation intermediate associated with hUNG2 has been proposed to be stabilized by the uracilate anion, an active-site aspartate, and the −2 phosphate moiety.[80,81] The lack of additional stabilization of the cationic sugar by the leaving group explains the larger role for D144 observed in the present work compared to that discussed for other glycosylases. Interestingly, a recent mutational study replaced D144 with glutamate and cysteine, and MutY retains activity as long as the pH maintains the anionic charge of the group.[30] Therefore, the charge of this residue is essential for MutY catalysis. The importance of charge has also been displayed for the helix-capping aspartate residue in hOgg1 using alternative mutations and experimental conditions.[82] Definitive evidence of similar pH effects on Asp/Glu to cysteine mutations could verify the relative importance of the conserved residue across the glycosylases. It is also significant to note that the strong interaction between D144 and the oxacarbenium cation leads to a stable intermediate that can rearrange to an exothermic intermediate if the water nucleophile partially dissociates from the active site. This stabilizing effect suggests that addition of a water molecule to the anomeric carbon may not occur until after adenine release.

General Glycosylase Mechanism. A general mechanism for monofunctional activity of the DNA glycosylases can be developed by comparing the results of this study with our previous investigations of hUNG2[60] and AAG.[53] As discussed in our previous work on hUNG2, as well as in the literature,[16,17,38,41,83,84] leaving group stabilization by the enzyme is essential for efficient catalysis of nucleoside deglycosylation via a dissociative S_N1 mechanism. As a result, enzymes that use an S_N1 mechanism (hUNG2 and MutY) contain many direct contacts through hydrogen-bond (and proton) donation to the nucleobase.[60] In contrast, AAG contains few such donating interactions with the leaving group, and an S_N2 mechanism was characterized for both neutral ethenoadenine (εA) and cationic (3-methyladenine) substrate.[53] These comparisons suggest that one may be able to estimate the relative dissociative nature of a glycosylase mechanism based on the number and type of interactions with the nucleobase leaving group.

In addition to leaving group activation, electrostatic stabilization of the oxacarbenium transition state and nucleophile activation are essential to glycosylase activity and are generally attributed to an active-site Asp/Glu residue.[16,17] Although the distance between the sugar and catalytic Asp/Glu is over 3.6 Å (d(C1′−O_{Asp}) = 3.624−4.258 Å) in the reactant for hUNG2 and AAG,[53,60] this distance is significantly reduced in the case of MutY (d(C1′−O_{Asp}) = 3.209 Å). In addition, only the MutY reactant places the aspartate directly below the sugar ring, while the Asp/Glu is closer to C2′ and O4′ in the hUNG2 and AAG active sites, respectively. This led to our newly proposed MutY mechanism, which involves mutual migration of the aspartate and the anomeric carbon in the sugar moiety. In contrast to some proposals in the literature,[16,17,80,85] our computational studies have found that the Asp/Glu residue is a very poor general base. In the case of hUNG2, another general base (histidine) can activate the nucleophile.[60] However, neither AAG nor MutY contain a second general base in the vicinity of the nucleophile. Although shuttling a proton to the leaving group could make up for the lack of a strong general base and has been proposed for AAG,[78] full proton transfer was not observed in our study when AAG acts on (neutral) εA,[53] which likely in part led to the preferred S_N2 pathway. Furthermore, a similar proton transfer is not possible during MutY activity since the nucleobase product is already neutral, and (in the case of MutY) hydrogen bound to a cationic (arginine) residue, which makes the departed substrate a very poor base. Therefore, the calculated barrier for addition of the water nucleophile to the sugar is larger than anticipated from experimental data for MutY but is consistent with hUNG2

dx.doi.org/10.1021/bi401310w | *Biochemistry* 2013, 52, 8753−8765

being significantly faster ($k_{deglyco}$ = 540 min^{-1})[86] than MutY ($k_{deglyco}$ = 12 ± 2 min^{-1}).[38] Thus, we believe that our computational approach can be used with confidence to gain information about other glycosylases for which less experimental data is available.

In summary, our calculations show that a computational protocol combining MD and detailed ONIOM reaction potential energy surfaces can reveal vital information about the glycosylase reaction catalyzed by MutY that is otherwise difficult to ascertain. More importantly, consideration of a crystal structure that likely more closely represents a reactant complex for the first time allows us to explain the experimentally observed significant dependence of the MutY reaction on the charged active-site aspartate residue, as well as propose and justify a larger role for the conserved Asp/Glu residue in the MutY reaction compared to the other glycosylases. Finally, our work has identified a catalytic role of Y126, namely, stabilization of a highly charged active site throughout the chemical step, which may also suggest a significant role for tyrosine in the reactions catalyzed by other DNA glycosylases or other enzymes containing, for example, tyrosine-glutamate dyads. As a result, our work suggests that future experimental studies should more closely investigate the role of active site tyrosine and conserved Asp/Glu residues in the mechanism of action of the DNA glycosylases, as well as other enzymes that facilitate nucleoside deglycosylation.

■ ASSOCIATED CONTENT

Supporting Information

Full computational details; parameters for modified nucleotides and iron−sulfur cluster; list of model contents and layer division; summary of solvation shells; hydrogen-bond occupancies for dA and E43, and D144; atom types for modified nucleotides and iron−sulfur cluster; occupancy of the first solvation shell; occupancy of E43−dA; occupancy of the D144 orientation and helix-capping interaction; occupancy of Y126−E43; overlay of crystal structure active sites; orientation of Y126; helix-capping orientation; occupancy of sugar pucker; occupancy of E188 conformation; electron density and alternate orientation for E188; reaction PES for the proton transfer reaction; important contacts for the standard hydrolysis and D144-catalyzed hydrolysis mechanisms; RMSD; electron density for Y126 and E43; DFT region of the activated reactants for all models and the stationary points for relaxed mechanisms; and full citations for refs 68, 71, and 72. This material is available free of charge via the Internet at http://pubs.acs.org.

■ AUTHOR INFORMATION

Corresponding Author

*Tel: 403-329-2323. Fax: 403-329-2057. E-mail: stacey.wetmore@uleth.ca.

Funding

We thank the Natural Sciences and Engineering Research Council of Canada (NSERC), the Canadian Research Chair Program, and the Canadian Foundation for Innovation (CFI) for financial support. J.L.K acknowledges NSERC (CGS-D) and the University of Lethbridge, while K.A.W. acknowledges NSERC (USRA), for student scholarships.

Notes

The authors declare no competing financial interest.

■ ACKNOWLEDGMENTS

Computational resources from the Upscale and Robust Abacus for Chemistry in Lethbridge (URACIL) and those provided by Westgrid and Compute/Calcul Canada are greatly appreciated.

■ ABBREVIATIONS

A, adenine; AlkA (AAG), alkyladenine−DNA glycosylase; BER, base excision repair; C, cytosine; DFT, density functional theory; DNA, deoxyribonucleaic acid; FdA, 2′-fluoro-dA; FLRC, fluorinated lesion recognition complex; hMYH, human MutY homologue; hOgg1, human 8-oxoguanine−DNA glycosylase; hUNG2 (UDG), human uracil−DNA glycosylase; LRC, lesion recognition complex; MAP, MYH-assisted polyposis; MD, molecular dynamics; MutM (FPG), formamido-purine DNA glycosylase; MutT, 8-oxoguanine nucleosidase; MutY, adenine−DNA glycosylase; NEIL1, endonuclease VIII-like DNA glycosylase; OG, 8-oxoguanine; ONIOM, our own N-layered integrated molecular orbital; PES, potential energy surface; QM, quantum mechanics; RMSD, root-mean-square deviation; T, thymine

■ REFERENCES

(1) Cadet, J., Douki, T., and Ravanat, J.-L. (2010) Oxidatively generated base damage to cellular DNA. *Free Radical Biol. Med. 49*, 9−21.

(2) Tsuzuki, T., Nakatsu, Y., and Nakabeppu, Y. (2007) Significance of error-avoiding mechanisms for oxidative DNA damage in carcinogenesis. *Cancer Sci. 98*, 465−470.

(3) Paz-Elizur, T., Sevilya, Z., Leitner-Dagan, Y., Elinger, D., Roisman, L. C., and Livneh, Z. (2008) DNA repair of oxidative DNA damage in human carcinogenesis: potential application for cancer risk assessment and prevention. *Cancer Lett. 266*, 60−72.

(4) Kryston, T. B., Georgiev, A. B., Pissis, P., and Georgakilas, A. G. (2011) Role of oxidative stress and DNA damage in human carcinogenesis. *Mutat. Res., Fundam. Mol. Mech. Mutagen. 711*, 193−201.

(5) Ziech, D., Franco, R., Pappa, A., and Panayiotidis, M. I. (2011) Reactive oxygen species (ROS) − induced genetic and epigenetic alterations in human carcinogenesis. *Mutat. Res., Fundam. Mol. Mech. Mutagen. 711*, 167−173.

(6) Evans, M. D., Dizdaroglu, M., and Cooke, M. S. (2004) Oxidative DNA damage and disease: induction, repair and significance. *Mutat. Res. 567*, 1−61.

(7) Halliwell, B. (2006) Oxidative Stress and neurodegeneration: where are we now? *J. Neurochem. 97*, 1634−1658.

(8) Tanrikulu, S., Dogru-Abbasoglu, S., Ozderya, A., Ademoglu, E., Karadag, B., Erbil, Y., and Uysal, M. (2011) The 8-oxoguanine DNA N-glycosylase 1 (hOGG1) Ser326Cys variant affects the susceptibility to Graves' disease. *Cell Biochem. Funct. 29*, 244−248.

(9) Dodson, M. L., and Lloyd, R. S. (2001) Backbone dynamics of DNA containing 8-oxoguanine: importance for substrate recognition by base excision repair glycosylases. *Mutat. Res., DNA Repair 487*, 93−108.

(10) Cheng, X. L., Kelso, C., Hornak, V., de los Santos, C., Grollman, A. P., and Simmerling, C. (2005) Dynamic behavior of DNA base pairs containing 8-oxoguanine. *J. Am. Chem. Soc. 127*, 13906−13918.

(11) Singh, S. K., Szulik, M. W., Ganguly, M., Khutsishvili, I., Stone, M. P., Marky, L. A., and Gold, B. (2011) Characterization of DNA with an 8-oxoguanine modification. *Nucleic Acids Res. 39*, 6789−6801.

(12) Markkanen, E., Hubscher, U., and van Loon, B. (2012) Regulation of oxidative dna damage repair: the adenine: 8-oxo-guanine problem. *Cell Cycle 11*, 1070−1075.

(13) Michaels, M. L., and Miller, J. H. (1992) The GO system protects organisms from the mutagenic effect of the spontaneous lesion 8-hydroxyguanine (7,8-dihydro-8-oxoguanine). *J. Bacteriol. 174*, 6321−6325.

(14) Lu, A. L., Li, X., Gu, Y., Wright, P. M., and Chang, D.-Y. (2001) Repair of oxidative DNA damage: mechanisms and functions. *Cell Biochem. Biophys. 35*, 141−170.
(15) Russo, M. T., De Luca, G., Degan, P., and Bignami, M. (2007) Different DNA repair strategies to combat the threat from 8-oxoguanine. *Mutat. Res. 614*, 69−76.
(16) Stivers, J. T., and Jiang, Y. L. (2003) A mechanistic perspective on the chemistry of DNA repair glycosylases. *Chem. Rev. 103*, 2729−2759.
(17) Berti, P. J., and McCann, J. A. B. (2006) Toward a detailed understanding of base excision repair enzymes: transition state and mechanistic analyses of N-glycoside hydrolysis and N-glycoside transfer. *Chem. Rev. 106*, 506−555.
(18) Sekiguchi, M., and Tsuzuki, T. (2002) Oxidative nucleotide damage: consequences and prevention. *Oncogene 21*, 8895−8904.
(19) Arczewska, K. D., and Kusmierek, J. T. (2007) Bacterial DNA repair genes and their eukaryotic homologues: 2. Role of bacterial mutator gene homologues in human disease. Overview of nucleotide pool sanitization and mismatch repair systems. *Acta Biochim. Pol. 54*, 435−457.
(20) Lu, A. L., Yuen, D. S., and Cillo, J. (1996) Catalytic mechanism and DNA substrate recognition of *Escherichia coli* MutY protein. *J. Biol. Chem. 271*, 24138−24143.
(21) Pope, M. A., Chmiel, N. H., and David, S. S. (2005) Insight into the functional consequences of hMYH variants associated with colorectal cancer: distinct differences in the adenine glycosylase activity and the response to AP endonucleases of Y150C and G365D murine MYH. *DNA Repair 4*, 315−325.
(22) Cheadle, J. P., and Sampson, J. R. (2007) MUTYH-associated polyposis: from defect in base excision repair to clinical genetic testing. *DNA Repair 6*, 274−279.
(23) Guan, Y., Manuel, R. C., Arvai, A. S., Parikh, S. S., Mol, C. D., Miller, J. H., Lloyd, S., and Tainer, J. A. (1998) MutY catalytic core, mutant and bound adenine structures define specificity for DNA repair enzyme superfamily. *Nat. Struct. Biol. 5*, 1058−1064.
(24) Wright, P. M., Yu, J. A., Cillo, J., and Lu, A. L. (1999) The active site of the *Escherichia coli* MutY DNA adenine glycosylase. *J. Biol. Chem. 274*, 29011−29018.
(25) Williams, S. D., and David, S. S. (2000) A single engineered point mutation in the adenine glycosylase MutY confers bifunctional glycosylase/AP lyase activity. *Biochemistry 39*, 10098−10109.
(26) Zharkov, D. O., Gilboa, R., Yagil, I., Kycia, J. H., Gerchman, S. E., Shoham, C., and Grollman, A. P. (2000) Role for lysine 142 in the excision of adenine from A:G mispairs by MutY DNA glycosylase of *Escherichia coli*. *Biochemistry 39*, 14768−14778.
(27) Chmiel, N. H., Livingston, A. L., and David, S. S. (2003) Insight into the functional consequences of inherited variants of the hMYH adenine glycosylase associated with colorectal cancer: complementation assays with hMYH variants and pre-steady-state kinetics of the corresponding mutated *E. coli* enzymes. *J. Mol. Biol. 327*, 431−443.
(28) Chepanoske, C. L., Lukianova, O. A., Lombard, M., Golinelli-Cohen, M. P., and David, S. S. (2004) A residue in MutY important for catalysis identified by photocross-linking and mass spectrometry. *Biochemistry 43*, 651−662.
(29) Livingston, A. L., Kundu, S., Pozzi, M. H., Anderson, D. W., and David, S. S. (2005) Insight into the roles of tyrosine 82 and glycine 253 in the *Escherichia coli* adenine glycosylase MutY. *Biochemistry 44*, 14179−14190.
(30) Brinkmeyer, M. K., Pope, M. A., and David, S. S. (2012) Catalytic contributions of key residues in the adenine glycosylase MutY revealed by pH-dependent kinetics and cellular repair assays. *Chem. Biol. 19*, 276−286.
(31) Lu, A. L., Tsaiwu, J. J., and Cillo, J. (1995) DNA determinants and substrate specificities of *Escherichia-coli* MutY. *J. Biol. Chem. 270*, 23582−23588.
(32) Bulychev, N. V., Varaprasad, C. V., Dorman, G., Miller, J. H., Eisenberg, M., Grollman, A. P., and Johnson, F. (1996) Substrate specificity of *Escherichia coli* MutY protein. *Biochemistry 35*, 13147−13156.
(33) Porello, S. L., Williams, S. D., Kuhn, H., Michaels, M. L., and David, S. S. (1996) Specific recognition of substrate analogs by the DNA mismatch repair enzyme MutY. *J. Am. Chem. Soc. 118*, 10684−10692.
(34) Chepanoske, C. L., Porello, S. L., Fujiwara, T., Sugiyama, H., and David, S. S. (1999) Substrate recognition by *Escherichia coli* MutY using substrate analogs. *Nucleic Acids Res. 27*, 3197−3204.
(35) Chepanoske, C. L., Langelier, C. R., Chmiel, N. H., and David, S. S. (2000) Recognition of the nonpolar base 4-methylindole in DNA by the DNA repair adenine glycosylase MutY. *Org. Lett. 2*, 1341−1344.
(36) Ohtsubo, T., Nishioka, K., Imaiso, Y., Iwai, S., Shimokawa, H., Oda, H., Fujiwara, T., and Nakabeppu, Y. (2000) Identification of human MutY homolog (hMYH) as a repair enzyme for 2-hydroxyadenine in DNA and detection of multiple forms of hMYH located in nuclei and mitochondria. *Nucleic Acids Res. 28*, 1355−1364.
(37) Chmiel, N. H., Golinelli, M. P., Francis, A. W., and David, S. S. (2001) Efficient recognition of substrates and substrate analogs by the adenine glycosylase MutY requires the C-terminal domain. *Nucleic Acids Res. 29*, 553−564.
(38) Francis, A. W., Helquist, S. A., Kool, E. T., and David, S. S. (2003) Probing the requirements for recognition and catalysis in FPG and MutY with nonpolar adenine isosteres. *J. Am. Chem. Soc. 125*, 16235−16242.
(39) Ushijima, Y., Tominaga, Y., Miura, T., Tsuchimoto, D., Sakumi, K., and Nakabeppu, Y. (2005) A functional analysis of the DNA glycosylase activity of mouse MUTYH protein excising 2-hydroxyadenine opposite guanine in DNA. *Nucleic Acids Res. 33*, 672−682.
(40) Livingston, A. L., O'Shea, V. L., Kim, T., Koo, E. T., and David, S. S. (2008) Unnatural substrates reveal the importance of 8-oxoguanine for *in vivo* mismatch repair by MutY. *Nat. Chem. Biol. 4*, 51−58.
(41) McCann, J. A. B., and Berti, P. J. (2008) Transition-state analysis of the DNA repair enzyme MutY. *J. Am. Chem. Soc. 130*, 5789−5797.
(42) Fromme, J. C., Banerjee, A., Huang, S. J., and Verdine, G. L. (2004) Structural basis for removal of adenine mispaired with 8-oxoguanine by MutY adenine DNA glycosylase. *Nature (London, U. K.) 427*, 652−656.
(43) Messick, T. E., Chmiel, N. H., Golinelli, M. P., Langer, M. R., Joshua-Tor, L., and David, S. S. (2002) Noncysteinyl coordination to the 4Fe-4S (2+) cluster of the DNA repair adenine glycosylase MutY introduced via site-directed mutagenesis. structural characterization of an unusual histidinyl-coordinated cluster. *Biochemistry 41*, 3931−3942.
(44) Manuel, R. C., Hitomi, K., Arvai, A. S., House, P. G., Kurtz, A. J., Dodson, M. L., McCullough, A. K., Tainer, J. A., and Lloyd, R. S. (2004) Reaction intermediates in the catalytic mechanism of *Escherichia coli* MutY DNA glycosylase. *J. Biol. Chem. 279*, 46930−46939.
(45) Lee, S., and Verdine, G. L. (2009) Atomic substitution reveals the structural basis for substrate adenine recognition and removal by adenine DNA glycosylase. *Proc. Natl. Acad. Sci. U.S.A. 106*, 18497−18502.
(46) Luncsford, P. J., Chang, D. Y., Shi, G. L., Bernstein, J., Madabushi, A., Patterson, D. N., Lu, A. L., and Toth, E. A. (2010) A structural hinge in eukaryotic MutY homologues mediates catalytic activity and Rad9-Rad1-Hus1 checkpoint complex interactions. *J. Mol. Biol. 403*, 351−370.
(47) Schroeder, G. K., and Wolfenden, R. (2007) Rates of spontaneous disintegration of DNA and the rate enhancements produced by DNA glycosylases and deaminases. *Biochemistry 46*, 13638−13647.
(48) Xu, D. G., and Guo, H. (2009) Quantum mechanical/molecular mechanical and density functional theory studies of a prototypical zinc peptidase (carboxypeptidase A) suggest a general acid-general base mechanism. *J. Am. Chem. Soc. 131*, 9780−9788.
(49) López-Canut, V., Roca, M., Bertrán, J., Moliner, V., and Tuñón, I. (2010) Theoretical study of phosphodiester hydrolysis in nucleotide pyrophosphatase/phosphodiesterase. environmental effects on the reaction mechanism. *J. Am. Chem. Soc. 132*, 6955−6963.

(50) Barnett, C. B., Wilkinson, K. A., and Naidoo, K. J. (2011) Molecular details from computational reaction dynamics for the cellobiohydrolase I glycosylation reaction. *J. Am. Chem. Soc. 133*, 19474−19482.
(51) Gómez, H., Polyak, I., Thiel, W., Lluch, J. M., and Masgrau, L. (2012) Retaining glycosyltransferase mechanism studied by QM/MM methods: lipopolysaccharyl-α-1,4-galactosyltransferase C transfers α-galactose via an oxocarbenium ion-like transition state. *J. Am. Chem. Soc. 134*, 4743−4752.
(52) Huang, W., Bushnell, E. A. C., Francklyn, C. S., and Gauld, J. W. (2011) The α-amino group of the threonine substrate as the general base during tRNA aminoacylation: a new version of substrate-assisted catalysis predicted by hybrid DFT. *J. Phys. Chem. A 115*, 13050−13060.
(53) Rutledge, L. R., and Wetmore, S. D. (2011) Modeling the chemical step utilized by human alkyladenine DNA glycosylase: a concerted mechanism aids in selectively excising damaged purines. *J. Am. Chem. Soc. 133*, 16258−16269.
(54) Alexandrova, A. N., Röthlisberger, D., Baker, D., and Jorgensen, W. L. (2008) Catalytic mechanism and performance of computationally designed enzymes for kemp elimination. *J. Am. Chem. Soc. 130*, 15907−15915.
(55) Lundberg, M., Kawatsu, T., Vreven, T., Frisch, M. J., and Morokuma, K. (2009) Transition states in a protein environment: ONIOM QM:MM modeling of isopenicillin N synthesis. *J. Chem. Theory Comput. 5*, 222−234.
(56) Hirao, H., and Morokuma, K. (2011) ONIOM(DFT:MM) Study of 2-hydroxyethylphosphonate dioxygenase: what determines the destinies of different substrates? *J. Am. Chem. Soc. 133*, 14550−14553.
(57) Ke, Z., Abe, S., Ueno, T., and Morokuma, K. (2012) Catalytic mechanism in artificial metalloenzyme: QM/MM study of phenylacetylene polymerization by rhodium complex encapsulated in apoferritin. *J. Am. Chem. Soc. 134*, 15418−15429.
(58) Tiwari, S., Agnihotri, N., and Mishra, P. C. (2011) Quantum theoretical study of cleavage of the glycosidic bond of 2′-deoxyadenosine: base excision-repair mechanism of DNA by MutY. *J. Phys. Chem. B 115*, 3200−3207.
(59) Brunk, E., Arey, J. S., and Rothlisberger, U. (2012) Role of environment for catalysis of the DNA repair enzyme MutY. *J. Am. Chem. Soc. 134*, 8608−8616.
(60) Przybylski, J. L., and Wetmore, S. D. (2011) A QM/QM investigation of the hUNG2 reaction surface: the untold tale of a catalytic residue. *Biochemistry 50*, 4218−4227.
(61) Bas, D. C., Rogers, D. M., and Jensen, J. H. (2008) Very fast prediction and rationalization of pK(a) values for protein-ligand complexes. *Proteins: Struct., Funct., Bioinf. 73*, 765−783.
(62) Li, H., Robertson, A. D., and Jensen, J. H. (2005) Very Fast Empirical Prediction and Rationalization of Protein pK(a) Values. *Proteins: Struct., Funct., Bioinf. 61*, 7040−7721.
(63) Olsson, M. H. M., Sondergaard, C. R., Rostkowski, M., and Jensen, J. H. (2011) PROPKA3: consistent treatment of internal and surface residues in empirical pK(a) predictions. *J. Chem. Theory Comput. 7*, 525−537.
(64) Sondergaard, C. R., Olsson, M. H. M., Rostkowski, M., and Jensen, J. H. (2011) Improved treatment of ligands and coupling effects in empirical calculation and rationalization of pK(a) values. *J. Chem. Theory Comput. 7*, 2284−2295.
(65) Wang, J., Wolf, R. M., Caldwell, J. W., Kollman, P. A., and Case, D. A. (2004) Development and testing of a general Amber force field. *J. Comput. Chem. 25*, 1157−1174.
(66) Hornak, V., Abel, R., Okur, A., Strockbine, B., Roitberg, A., and Simmerling, C. (2006) Comparison of multiple AMBER force fields and development of improved protein backbone parameters. *Proteins: Struct., Funct., Bioinf. 65*, 712−725.
(67) Wang, J., Wang, W., Kollman, P. A., and Case, D. A. (2006) Automatic atom type and bond type perception in molecular mechanical calculations. *J. Mol. Graphics Modell. 25*, 247−260.
(68) Frisch, M. J., Trucks, G. W., Schlegel, H. B., Scuseria, G. E., Robb, M. A., Cheeseman, J. R., Scalmani, G., Barone, V., Mennucci, B., Petersson, G. A., et al.. (2009) *Gaussian 09*, revision A.02, Gaussian, Inc., Wallingford, CT.
(69) Dupradeau, F.-Y., Pigache, A., Zaffran, T., Savineau, C., Lelong, R., Grivel, N., Lelong, D., Rosanski, W., and Cieplak, P. (2010) The R.E.D. tools: advances in RESP and ESP charge derivation and force field library building. *Phys. Chem. Chem. Phys. 12*, 7821−7839.
(70) Smith, D. M. A., Xiong, Y. J., Straatsma, T. P., Rosso, K. M., and Squier, T. C. (2012) Force-field development and molecular dynamics of NiFe hydrogenase. *J. Chem. Theory Comput. 8*, 2103−2114.
(71) Case, D. A., Darden, T. A., Cheatham, I., Simmerling, C. L., Wang, J., Duke, R. E., Luo, R., Walker, R. C., Zhang, W., Merz, K. M., et al. (2012) *AMBER 12*, University of California, San Francisco, CA.
(72) Case, D. A., Darden, T. A., Cheatham, I., Simmerling, C. L., Wang, J., Duke, R. E., Luo, R., Crowley, M., Walker, R. C., Zhang, W., et al. (2010) *AMBER 11*, University of California, San Francisco, CA.
(73) Rios-Font, R., Rodriguez-Santiago, L., Bertran, J., and Sodupe, M. (2007) Influence of N7 protonation on the mechanism of the N-glycosidic bond hydrolysis in 2′-deoxyguanosine. A theoretical study. *J. Phys. Chem. B 111*, 6071−6077.
(74) Zheng, Y., Xue, Y., and Yan, S. G. (2008) The effects of oxidation and protonation on the N-glycosidic bond stability of 8-oxo-2′-deoxyguanosine: DFT study. *THEOCHEM 860*, 52−57.
(75) Zheng, Y., Xue, Y., and Yan, G. S. (2009) The influences of oxidation and cationization on the n-glycosidic bond stability of 8-oxo-2′-deoxyadenosine - a theoretical study. *J. Theor. Comput. Chem. 8*, 1253−1264.
(76) McConnell, T. L., Wheaton, C. A., Hunter, K. C., and Wetmore, S. D. (2005) Effects of hydrogen bonding on the acidity of adenine, guanine, and their 8-oxo derivatives. *J. Phys. Chem. A 109*, 6351−6362.
(77) McCann, J. A. B., and Berti, P. J. (2003) Adenine release is fast in MutY-catalyzed hydrolysis of G:A and 8-oxo-G:A DNA mismatches. *J. Biol. Chem. 278*, 29587−29592.
(78) Lau, A. Y., Wyatt, M. D., Glassner, B. J., Samson, L. D., and Ellenberger, T. (2000) Molecular basis for discriminating between normal and damaged bases by the human alkyladenine glycosylase, AAG. *Proc. Natl. Acad. Sci. U.S.A. 97*, 13573−13578.
(79) Lingaraju, G. M., Davis, C. A., Setser, J. W., Samson, L. D., and Drennan, C. L. (2011) Structural basis for the inhibition of human alkyladenine DNA glycosylase (AAG) by 3,N4-ethenocytosine-containing DNA. *J. Biol. Chem. 286*, 13205−13213.
(80) Dinner, A. R., Blackburn, G. M., and Karplus, M. (2001) Uracil-DNA glycosylase acts by substrate autocatalysis. *Nature (London, U. K.) 413*, 752−755.
(81) Parker, J. B., and Stivers, J. T. (2008) Uracil DNA Glycosylase: revisiting substrate-assisted catalysis by DNA phosphate anions. *Biochemistry 47*, 8614−8622.
(82) Norman, D. P. G., Chung, S. J., and Verdine, G. L. (2003) Structural and biochemical exploration of a critical amino acid in human 8-oxoguanine glycosylase. *Biochemistry 42*, 1564−1572.
(83) Drohat, A. C., Xiao, G. Y., Tordova, M., Jagadeesh, J., Pankiewicz, K. W., Watanabe, K. A., Gilliland, G. L., and Stivers, J. T. (1999) Heteronuclear NMR and crystallographic studies of wild-type and H187Q *Escherichia coli* uracil DNA glycosylase: electrophilic catalysis of uracil expulsion by a neutral histidine 187. *Biochemistry 38*, 11876−11886.
(84) Drohat, A. C., and Stivers, J. T. (2000) *Escherichia coli* uracil DNA glycosylase: NMR characterization of the short hydrogen bond from His187 to uracil O2. *Biochemistry 39*, 11865−11875.
(85) Fromme, J. C., Bruner, S. D., Yang, W., Karplus, M., and Verdine, G. L. (2003) Product-assisted catalysis in base-excision DNA repair. *Nat. Struct. Biol. 10*, 204−211.
(86) Slupphaug, G., Eftedal, I., Kavli, B., Bharati, S., Helle, N. M., Haug, T., Levine, D. W., and Krokan, H. E. (1995) Properties of a recombinant human uracil-DNA glycosylase from the *Ung* gene and evidence that *Ung* encodes the major uracil-DNA glycosylase. *Biochemistry 34*, 128−138.